

Giant spin-polarized current in a Dirac fermion system at cyclotron resonance

P. Olbrich,¹ C. Zoth,¹ P. Vierling,¹ K.-M. Dantscher,¹ G.V. Budkin,² S.A. Tarasenko,²
V.V. Bel'kov,² D.A. Kozlov,³ Z.D. Kvon,³ N.N. Mikhailov,³ S.A. Dvoretzky,³ and S.D. Ganichev¹
¹Terahertz Center, University of Regensburg, 93040 Regensburg, Germany
²A.F. Ioffe Physical-Technical Institute, Russian Academy of Sciences, 194021 St. Petersburg, Russia and
³Institute of Semiconductor Physics, Novosibirsk, Russia

We report on the observation of the giant spin-polarized photocurrent in HgTe/HgCdTe quantum well (QW) of critical thickness at which a Dirac spectrum emerges. Exciting QW of 6.6 nm width by terahertz (THz) radiation and sweeping magnetic field we detected a resonant photocurrent. Remarkably, the position of the resonance can be tuned from negative (-0.4 T) to positive (up to 1.2 T) magnetic fields by means of optical gating. The photocurrent data, accompanied by measurements of radiation transmission as well as Shubnikov-de Haas and quantum Hall effects, give an evidence that the enhancement of the photocurrent is caused by cyclotron resonance in a Dirac fermion system. The developed theory shows that the current is spin polarized and originates from the spin dependent scattering of charge carriers heated by the radiation.

PACS numbers: 73.21.Fg, 72.25.Fe, 78.67.De, 73.63.Hs

The electron *dc* transport in semiconductor systems with massless Dirac fermions has recently moved into the focus of modern research yielding challenging fundamental concepts as well as holding a great potential for applications [1–3]. The linear energy spectrum allows the observation of quantum kinetic effects and, on the other hand, gives a rise to a new class of phenomena absent in materials with parabolic dispersion. The massless Dirac fermions are realized in graphene [4], at surface states of bulk topological insulators (TI) [1–3, 5], in edge channels of two-dimensional TI [6] as well as in HgTe/HgCdTe QWs of critical thickness [7–9]. In the latter case and TIs, the linear energy spectrum is formed by strong spin-orbit interaction which locks the orbital motion of carriers with their spins. The interest in Dirac fermions in such materials resulted in theoretical consideration and observation of such fundamental physical phenomena as the quantum spin Hall effect [6, 7, 10–12], quantum Hall effect (QHE) on topological surface states [13], magneto-electric effect [14, 15], and quantum interference effects [16–21]. A considerable attention has been also given to the *nonlinear* high frequency (HF) transport phenomena. A plethora of such effects has been treated theoretically, including photogalvanics in TI systems [22–25], and second harmonic generation (SHG) [26] as well as radiation-induced QHE [27] and topological states [28]. While a great number of proposals have been published in the last two years, the number of experiments on the topic is limited so far by a few publications reporting the observation of SHG and photogalvanic effects in 3D TIs induced by near infrared radiation [26, 29–31].

Here, we report on the observation of a *dc* current excited by THz radiation in HgTe/HgCdTe QWs of critical thickness. We show that the current is giantly enhanced at cyclotron resonance (CR) being a few orders of magnitude higher than THz radiation excited photocurrents

detected in other non-magnetic QW structures. Due to the non-equidistant energy separation of Landau levels in systems with linear electron dispersion, the CR position is tuned by the variation of carrier density applying optical gate. The microscopic origin of the current is discussed in terms of the cyclotron motion, spin-dependent scattering and Zeeman splitting. We show that the current is spin-polarized and its enhancement comes from constructively contributing three factors: strong spin-orbit coupling, large *g*-factor in HgTe/HgCdTe QWs, and efficient radiation absorption at CR.

The experiments are carried out on (013)-oriented HgTe/Hg_{0.3}Cd_{0.7}Te QWs [32]. Single QW samples with widths, L_w , of 6.6 nm, and 21 nm and mobilities about $10^5 \text{ cm}^2/(\text{V}\cdot\text{s})$ at $T = 4.2 \text{ K}$ are investigated. The structures cross section is shown in Fig. 1(a). Eight ohmic contacts have been prepared at the corners and in the middle of the edges of $5 \times 5 \text{ mm}^2$ samples. Magneto-transport measurements show well pronounced Shubnikov-de Haas oscillations and QHE plateaus, see Fig. 1(c). To achieve a controllable variation of the carrier density we applied optical gating using the persistent photoconductivity effect well known for HgTe/HgCdTe QWs [9, 33, 34]. We illuminate the sample by red light emitting diode for a time t_i resulting in a change of the carrier density (type) which could be restored by heating the sample above $T \approx 150 \text{ K}$. The carrier densities measured for different t_i used in experiments are given in Table I.

For photocurrent excitation we apply a *cw* CH₃OH laser emitting a radiation with frequency $f = 2.54 \text{ THz}$ (wavelength $\lambda = 118 \mu\text{m}$) [35]. The radiation with power $P \approx 10 \text{ mW}$ is focused in a spot of about 1.5 mm diameter and modulated at 800 Hz. Right (σ^+) and left (σ^-) handed circularly polarized light is obtained by a $\lambda/4$ -plate. The experimental geometry is sketched in Fig. 1(b). In (013)-oriented QWs, excitation by normally incident THz radiation results in a photogalvanic

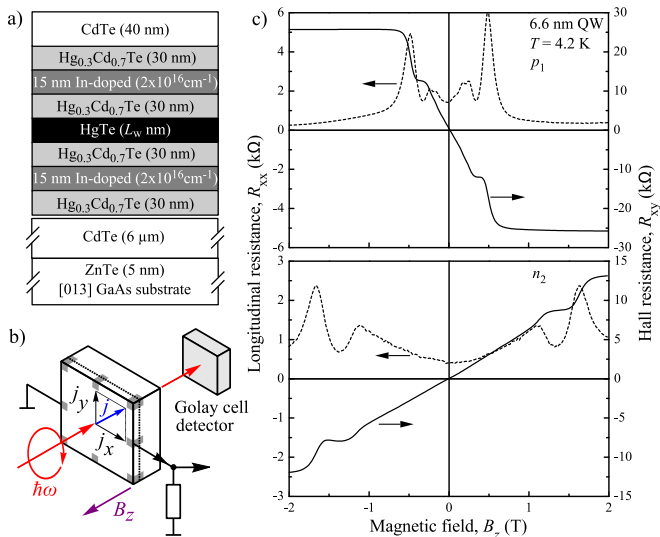


FIG. 1: (a) Cross section of the investigated structures. (b) Experimental set up used for the photocurrent and transmission measurements. (c) Magneto-transport data obtained in the van der Pauw geometry for 6.6 nm HgTe/HgCdTe QW sample without (top) and with (bottom) optical gating. The change of slope in the Hall signal indicates that initially p -type sample becomes n -type due to optical gating.

current even at $B_z = 0$ [36, 37], see Supplementary Materials. Owing low symmetry of QW, the photocurrent has no predefined direction and its magnitude, $j = \sqrt{j_x^2 + j_y^2}$, can be deduced by measuring the signals along two orthogonal directions [38]. The current-induced photovoltages $U_{x,y}$ are picked up across a 1 M Ω load resistor applying lock-in technique. The magnetic field B_z up to 4 T is applied normal to the QW plane. The photocurrent studies are accompanied by optical transmission, see Fig. 1(b), and magneto-transport experiments.

We start with the data obtained on the 6.6 nm QW, which should have a close to linear dispersion [9, 21]. Exciting the sample with right-handed circularly polarized radiation and sweeping magnetic field we observed a strong resonant photocurrent at $B_c = -0.42$ T, see Fig. 2. The signal at the resonance is more than two orders of magnitude higher than that detected at $B_z = 0$. By changing the carrier type from hole to electron one the resonance jumps from negative to positive B_z and

TABLE I: Sample parameters measured at $T = 4.2$ K.

	L_w , nm	illum.	density, $\text{cm}^{-2}10^{10}$	E_F , meV
p_1	6.6	-	1.5	15
n_1	6.6	+	3.4	21
n_2	6.6	+	11.0	39
n_3	21.0	-	18.0	15
n_4	21.0	+	24.0	21

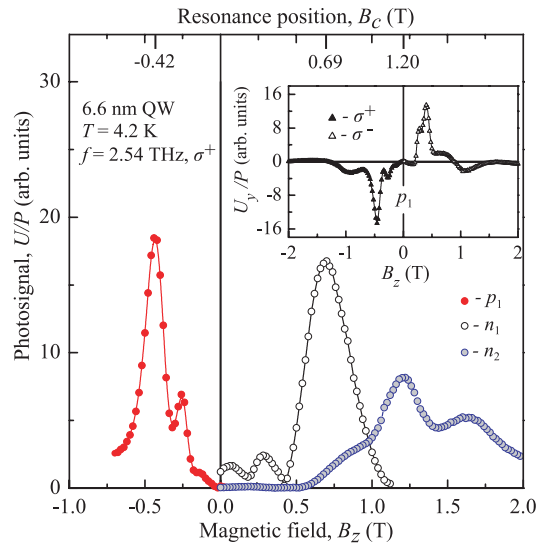


FIG. 2: Signal normalized by the radiation power U/P excited by σ^+ radiation vs. B_z . The data are shown for magnetic fields lower than the full quantization limit [39]. The inset shows data for σ^+ and σ^- light.

moves towards higher field, being now for the electron density $n_1 \approx 2 \times p_1$ at $B_c = +0.69$ T. Remarkably, at further increase in the electron density, the resonance position drifts to even higher B_c , being 1.2 T for $n_2 \approx 3 \times n_1$, see Fig. 2. Switching the radiation helicity from σ^+ to σ^- changes the current sign and mirrors the results with respect to the magnetic field polarity, as shown for p -type conductivity in the inset in Fig. 2. The above behavior is observed for the temperature range from 4.2 up to 150 K. The resonances are detected in the transmission measurements as well. The data for different carrier densities (type) are shown in Fig. 3 demonstrating a good correlation between the positions of the dip in the transmissivity and the resonant photocurrent.

Resonant photocurrents are also detected for the 21 nm QWs, a structure characterized by a nearly parabolic dispersion. Photocurrent (see Fig. 4) and transmission measurements (see Fig. 3) clearly show that the resonance position in these QWs is shifted to much higher magnetic fields $B_c \approx 3$ T. Furthermore, the resonance field now only slightly depends on the carrier density

The observed coincidence of peak positions in the photocurrent and transmissivity unambiguously proves that the resonant current is caused by CR [40]. This is also supported by the fact that for a fixed radiation helicity the resonances in the photocurrent and transmissivity are detected for one polarity of magnetic field only. The striking fact is that, depending on optical gating, the resonance for QWs with $L_w = 6.6$ nm is detected for negative as well as for positive magnetic field and its peak position drastically depends on the Fermi level. These results are in agreement with Ref. [9] which concludes that the energy dispersion in similar structures is close to lin-

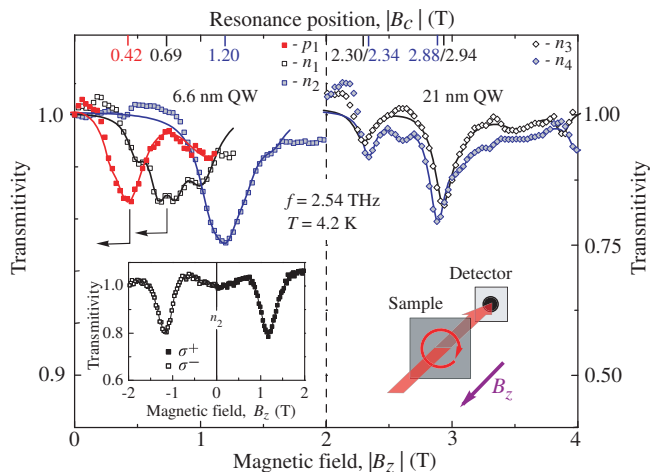


FIG. 3: Transmissivity of circularly polarized light as a function of the magnetic field modulus, $|B_z|$. Full lines are fits by a superposition of Lorentz functions. The inset shows the data obtained for σ^+ and σ^- light for the $L_w = 6.6$ nm samples.

ear. Such an electron spectrum lacks the band gap and, therefore, allows an easy transition from n - to p -type conductivity, as proved in transport and CR experiments, see Figs. 1-3. Furthermore, recent study of gated Hall bar 6.6 nm QWs samples prepared from the same batch, as samples studied here, manifests a weak localization effects even in the vicinity of Dirac point giving an additional proof for existence of gapless dispersion in these QWs [21]. As a matter of fact, the cyclotron frequency in a system with linear dispersion depends strongly on the Fermi energy - a characteristic behavior observed in our 6.6 nm sample. Indeed, the cyclotron frequency is described by the well known expression $\omega_c = |eB_z|/m_c c$, where e is the carrier charge, c is the speed of light, and m_c is the effective cyclotron mass at the Fermi energy. The latter, given by $m_c = p_F/(dE_F/dp_F)$ with p_F being the Fermi momentum, yields $m_c = E_F/v^2$ for a system with linear dispersion characterized by a constant velocity v . Taking $E_F = \sqrt{2\pi n}(\hbar v)$ into account, we obtain for the CR position $|B_c| = \sqrt{2\pi n}(c\hbar\omega)/|ev|$. From the resonance positions measured for electron densities n_1 and n_2 (Fig. 2) we find that the electron Fermi velocity is almost constant, being equal to 7.2×10^5 m/s. The value is in a good agreement with the electron velocity for 2D Dirac fermions in HgTe/HgCdTe QWs of critical thickness, $v = 6.3 \times 10^5$ m/s, obtained from the energy spectrum calculated in Ref. [8]. The hole velocity, deduced from our data for the density p_1 , is also close to this value (7.5×10^5 m/s). Note that the obtained values are close to the carrier velocity in graphene (10^6 m/s [4]). The substantially higher resonance field in 21 nm QWs as well as the observed weak dependence of its position on the electron density correspond to the CR behavior in HgTe/HgCdTe QWs characterized by a nearly parabolic

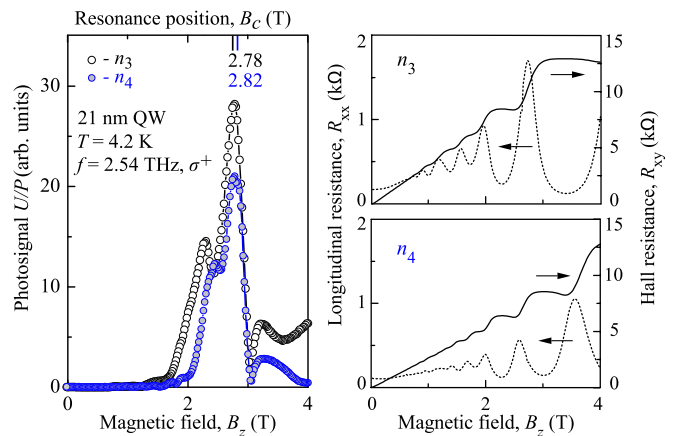


FIG. 4: Left panel: Magnetic field dependence of the signal U/P excited by σ^+ light in the 21 nm sample. Right panel shows the magneto-transport data.

dispersion with large Zeeman splitting [33, 34, 41–44].

Now we turn to the microscopic origin of the current generation at cyclotron resonance. The fact that the current is excited at normal incidence of radiation implies that it is inherently related to asymmetry of carrier relaxation (excitation) in \mathbf{k} -space in (013)-oriented QWs of low spatial symmetry [45]. In HgTe/HgCdTe QWs with known strong spin-orbit coupling and enhanced magnetic properties, the most likely candidate responsible for the microscopic origin of the asymmetry is spin-orbit coupling, in particular, spin-dependent scattering. The latter is a known fact for other III-V heterostructures [46, 47]. We consider the resonant absorption of THz radiation, which leads to the strong electron (hole) gas heating. The resulting steady-state non-equilibrium carrier distribution is formed by the energy gain due to the radiation absorption, electron-electron collisions thermalizing the electron gas, and the energy loss due to emission of phonons. The matrix element of electron scattering by phonon contains asymmetric spin-dependent terms (odd in the electron wave vector), which are similar to the Rashba and Dresselhaus spin-orbit terms in the energy dispersion [48]. Due to the spin-dependent part of the electron-phonon interaction, the energy relaxation of carriers in the spin cones is asymmetric and the relaxation rates for positive and negative wave vectors, say in x -direction, are different [49]. The asymmetry causes imbalance in the carrier distribution in \mathbf{k} -space and, hence, electron fluxes, see Fig. 5(b). The latter have opposite directions in the spin-up and spin-down cones. As, besides the cyclotron motion, the magnetic field splits the spin cones due to the Zeeman effect, one of the cones is preferentially populated compared to the other. Consequently, the fluxes in the spin cones are unbalanced, and a net electric current emerges. This process is sketched in Fig. 5 and, besides the linear dispersion, is alike that known for other non-magnetic QW

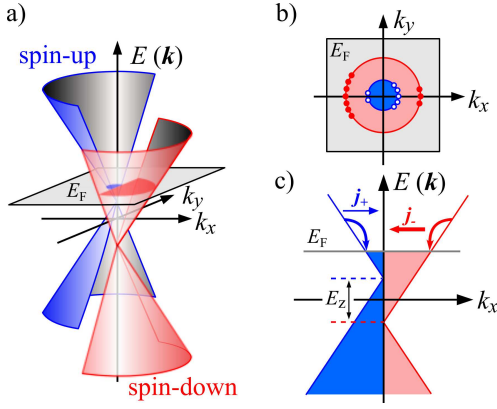


FIG. 5: Microscopic model. (a) Energy dispersion with spin-up (left, blue) and spin-down (right, red) cones shifted due to Zeeman effect to higher and lower energies, respectively. (b) Non-equilibrium carrier distribution at Fermi energy caused by the spin-dependent scattering. Full and open circles sketch the electron distribution in \mathbf{k} -space. (c) Energy relaxation of an electron gas heated as a result of the CR absorption. Due to the spin dependent scattering, the relaxation rates for electrons with positive and negative \mathbf{k} are different. Bent arrows show schematically a predominant energy relaxation in the spin-up (left) and spin-down (right) cones. The scattering asymmetry within each cone results in the oppositely directed fluxes \mathbf{j}_+ and \mathbf{j}_- shown by horizontal arrows. As due to the Zeeman effect the spin-down cone is larger populated, the flux \mathbf{j}_- is stronger than \mathbf{j}_+ and a dc electric current emerges.

structures [46, 47]. Obviously, the current magnitude is proportional to the radiation absorption, the strength of spin-orbit coupling, and the Zeeman splitting. The absorption is strongly enhanced in HgTe/HgCdTe QWs at the CR condition, resulting in the giant photocurrent observed in the experiments. While the models of the current formation for QWs with linear and parabolic dispersions are similar, the position of CR and its behavior upon variation of the Fermi energy are different. In particular, for a fixed radiation frequency, the cyclotron frequency is almost independent of the carrier density in QWs with nearly parabolic spectrum. By contrast, for QWs with linear spectrum, it drastically depends on the carrier density and for circularly polarized light may even change its sign in the same structure.

Following the model above, we now develop the quasi-classical theory of the effect. In this approach, the electron fluxes in the cones are given by $\mathbf{j}_s = e \sum_{\mathbf{k}} \mathbf{v} \delta f_{s\mathbf{k}}$, where $\delta f_{s\mathbf{k}}$ is the anisotropic part of the distribution function to be found from the kinetic equation, s is the index enumerating the Dirac cones. Here, $s = +$ corresponds to the cone formed from the states $|E1, +1/2\rangle = f_1(z)|\Gamma_6, +1/2\rangle + f_4(z)|\Gamma_8, +1/2\rangle$ and $|H1, +3/2\rangle = f_3(z)|\Gamma_8, +3/2\rangle$, $s = -$ corresponds to the cone formed from the states $|E1, -1/2\rangle = f_1(z)|\Gamma_6, -1/2\rangle + f_4(z)|\Gamma_8, -1/2\rangle$ and $|H1, -3/2\rangle = f_3(z)|\Gamma_8, -3/2\rangle$, with $f_1(z)$, $f_3(z)$, and $f_4(z)$ being the

envelope functions [7].

We consider that at low temperatures, relevant to the experimental conditions, the momentum relaxation of carriers is limited by elastic scattering from static defects while the energy relaxation is governed by deformation interaction with bulk acoustic phonons. The spin-dependent asymmetry of electron-phonon interaction in (013)-grown QWs is caused by the strain-induced coupling between the Γ_6 and Γ_8 band states [50–52] and deviation of the QW plane from the (001) plane by the angle $\theta \approx 18.4^\circ$. Then, for the linear electron dispersion in QWs with symmetric confinement potential, the resulting fluxes have the form (see Supplementary Material)

$$j_{\pm,x} = \mp \frac{|e|v \sin 2\theta}{2\sqrt{2}} \frac{n_{\pm}}{n} \left(\frac{d}{dE_F} \frac{\omega_c \tau_p^2}{1 + (\omega_c \tau_p)^2} \right) \xi I \eta, \quad (1)$$

$$j_{\pm,y} = \mp \frac{ev \sin 2\theta}{2\sqrt{2}} \frac{n_{\pm}}{n} \left(\frac{d}{dE_F} \frac{\tau_p}{1 + (\omega_c \tau_p)^2} \right) \xi I \eta.$$

Here $x \parallel [100]$ and $y \parallel [03\bar{1}]$ are the in-plane axes, n_{\pm} are the carrier densities in the cones, $n = n_+ + n_-$, τ_p is the momentum relaxation time, I is the radiation intensity, η is the free-carrier absorbance, ξ is a dimensionless parameter,

$$\xi = \frac{\int_{-\infty}^{+\infty} \Xi_{cv} Z_{13} (\Xi_c Z_{11} + \Xi_v Z_{33} + \Xi_v Z_{44}) q_z^2 dq_z}{\int_{-\infty}^{+\infty} [(\Xi_c Z_{11} + \Xi_v Z_{44})^2 + (\Xi_v Z_{33})^2] q_z^2 dq_z},$$

$Z_{ij} = \int_{-\infty}^{+\infty} f_i(z) f_j(z) \exp(iq_z z) dz$, Ξ_c and Ξ_v are the deformation-potential constants in the bands Γ_6 and Γ_8 , respectively, and Ξ_{cv} is the interband deformation-potential constant [51, 52].

For the circularly polarized radiation η in the vicinity of CR has the form

$$\eta = \frac{2e^2 E_F}{c \hbar^2 n_{\omega}} \frac{\tau_p}{1 + (\omega - \omega_c)^2 \tau_p^2}, \quad (2)$$

where n_{ω} is the refractive index. Assuming that the magnetic field splits the electron states due to the Zeeman effect but does not affect the scattering and taking into account that in experiment $\omega_c \tau_p \gg 1$, we estimate the net electric current $\mathbf{j} = \mathbf{j}_+ + \mathbf{j}_-$ as

$$\mathbf{j} = \frac{c \sin 2\theta}{2\sqrt{2}v} \frac{g\mu_0}{E_F} \xi I \eta, \quad (3)$$

where μ_0 is the Bohr magneton. Following the spectral behavior of the absorbance η the current \mathbf{j} exhibits a sharp peak at CR, whose position depends on the Fermi energy, in accordance with the experiment, see Fig. 2.

To summarize, we demonstrate that CR absorption by Dirac fermions in HgTe/HgCdTe QWs of critical thickness results in a resonant spin polarized electric current. The effect is very general and can be observed

in other Dirac fermion systems with a strong spin orbit coupling, e.g., surface states in 3D topological insulators like Bi_2Se_3 and Bi_2Te_3 . For the latter case such a study is of especial interest, because these crystals are centrosymmetric and, due to symmetry reasons, the photocurrent emerges only at surface. Consequently, it provides a unique selective access to fine details of their band structure like, e.g., effective mass and group velocity, as well as to the spin transport and spin-dependent scattering anisotropy [53, 54]. Finally, large resonant currents detected at low magnetic fields, about 0.5 T for 2.5 THz, indicate that HgTe/HgCdTe QWs of critical thickness are a good candidate for frequency selective CR-assisted detectors similar to that based on photoconductivity in bulk InSb [55], but operating at about 10 times lower magnetic fields.

We acknowledge useful discussions with R. Winkler and E. G. Novik. The support from the DFG, the Linkage Grant of IB of BMBF at DLR, RFBR, RF President grant MD-2062.2012.2, and the ‘‘Dynasty’’ Foundation is gratefully acknowledged.

-
- [1] M. Z. Hasan and C. L. Kane, *Rev. Mod. Phys.* **82**, 3045 (2010).
- [2] J. E. Moore, *Nature* **464**, 194 (2010).
- [3] S. C. Zhang *et al.*, *Rev. Mod. Phys.* **83**, 1057 (2011).
- [4] A. H. Castro Neto *et al.*, *Rev. Mod. Phys.* **81**, 109 (2009).
- [5] B. A. Volkov and O. A. Pankratov, *JETP Lett.* **42**, 178 (1985).
- [6] M. S. König *et al.*, *Science* **318**, 766 (2007).
- [7] B. A. Bernevig, T. L. Hughes and S. C. Zhang, *Science* **314**, 1757 (2006).
- [8] B. Büttner *et al.*, *Nature Phys.* **7**, 418 (2011).
- [9] Z. D. Kvon *et al.*, *JETP Lett.* **94**, 816 (2011).
- [10] C. L. Kane and E. J. Mele, *Phys. Rev. Lett.* **95**, 146802 (2005).
- [11] A. Roth *et al.*, *Science* **325**, 294 (2009).
- [12] D. Hsieh *et al.*, *Nature* **452**, 970 (2008).
- [13] C. Brüne *et al.*, *Phys. Rev. Lett.* **106**, 126803 (2011).
- [14] X. L. Qi, T. L. Hughes and S. C. Zhang, *Phys. Rev. B* **78**, 195424 (2008).
- [15] A. M. Essin, J. E. Moore, and D. Vanderbilt, *Phys. Rev. Lett.* **102**, 146805 (2009).
- [16] J. G. Checkelsky *et al.*, *Phys. Rev. Lett.* **103**, 246601 (2009).
- [17] H. Peng *et al.*, *Nature Mat.* **9**, 225 (2010).
- [18] J. Chen *et al.*, *Phys. Rev. Lett.* **105**, 176602 (2010).
- [19] H. Z. Lu, J. Shi and S. Q. Shen, *Phys. Rev. Lett.* **107**, 076801 (2011).
- [20] M. Liu *et al.*, *Phys. Rev. Lett.* **108**, 036805 (2012).
- [21] D. A. Kozlov *et al.*, *JETP Lett.* **96**, 730 (2012).
- [22] P. Hosur, *Phys. Rev. B* **83**, 035309(2011).
- [23] B. Dora, J. Cayssol, F. Simon, and R. Moessner, *Phys. Rev. Lett.* **108**, 056602 (2012).
- [24] Q. S. Wu *et al.*, *Physica E* **44**, 895 (2012).
- [25] Y. G. Semenov X. Li and K. W. Kim, arXiv 1208.2619 (2012).
- [26] J. W. McIver *et al.*, *Phys. Rev. B* **86**, 035327 (2012).
- [27] T. Kitagawa, T. Oka, A. Brataas, L. Fu, and E. Demler, *Phys. Rev. B* **84**, 235108 (2011).
- [28] N. H. Lindner G. Refael and V. Galitski, *Nature Phys.* **7**, 490 (2011).
- [29] D. Hsieh *et al.*, *Phys. Rev. Lett.* **106**, 057401 (2011).
- [30] J. W. McIver *et al.*, *Nature Nanotech.* **7**, 96 (2012).
- [31] C. Kastl *et al.*, arXiv:1210.4743v1 (2012).
- [32] Z. D. Kvon *et al.*, *Low Temp. Phys.* **35**, 6 (2009).
- [33] A. V. Ikonnikov *et al.*, *Semicond. Sci. Technol.* **26**, 125011 (2011).
- [34] M. S. Zholudev *et al.*, *Nanoscale Res. Lett.* **7**, 534 (2012).
- [35] Z. D. Kvon *et al.*, *Physica E* **40**, 1885 (2008).
- [36] S. D. Ganichev, E. L. Ivchenko, and W. Prettl, *Physica E* **14**, 166 (2002).
- [37] S. D. Ganichev and W. Prettl, *Intense Terahertz Excitation of Semiconductors* (Oxford Univ. Press, 2006).
- [38] B. Wittmann *et al.*, *Semicond. Sci. Technol.* **25**, 095005 (2010).
- [39] Our results reveal that for carrier densities p_1 [Fig. 1(a)] and n_1 (not shown) 2D system becomes fully quantized at low B_z so that R_{xy} approaches h/e^2 for B_z above 0.6 T and 1.2 T for densities p_1 and n_1 , respectively.
- [40] The data contain small side peaks, which may originate from the spin-flip CR in QWs with strong spin-orbit coupling and Zeeman splitting [42–44].
- [41] J. R. Meyer *et al.*, *J. Vac. Sci. Technol.* **B10**, 1582 (1992).
- [42] M. von Truchsess *et al.*, *J. Cryst. Growth* **159**, 1104 (1996).
- [43] M. Schultz *et al.*, *J. Cryst. Growth* **184/185**, 1180 (1998).
- [44] K. E. Spirin *et al.*, *JETP Lett.* **92**, 63 (2010).
- [45] E. L. Ivchenko, *Optical Spectroscopy of Semiconductor Nanostructures* (Alpha Science, 2005).
- [46] S. D. Ganichev, *et al.*, *Nature Phys.* **2**, 609 (2006).
- [47] V. V. Bel’kov, and S. D. Ganichev, *Semicond. Sci. Technol.* **23**, 114003 (2008).
- [48] *Spin Physics in Semiconductors*, ed. M. I. Dyakonov (Springer, 2008).
- [49] (013)-grown QWs belong to the C_1 point group. Thus, the coupling between the components of \mathbf{k} and spin vector is not predefined by symmetry.
- [50] G. E. Pikus, V. A. Marushchak, and A. N. Titkov, *Sov. Phys. Semicond.* **22**, 115 (1988).
- [51] E. L. Ivchenko and S. A. Tarasenko, *JETP* **99**, 379 (2004).
- [52] S. A. Tarasenko, *Semicond.* **42**, 967 (2008).
- [53] S. Giglberger *et al.*, *Phys. Rev. B* **75** 035327 (2007).
- [54] M. Kohda *et al.*, *Phys. Rev. B* **86**, 081306 (2012).
- [55] E. R. Brown, M. J. Wengler, and T. G. Phillips *J. Appl. Phys.* **58**, 2051 (1985).

SUPPLEMENTARY MATERIAL

PHOTO GALVANIC EFFECTS AT ZERO MAGNETIC FIELD

Illuminating our (013)-oriented QW structures with normally incident THz radiation we observed a *dc* electric current even in the absence of magnetic field. Figure 6 shows the dependence of the photosignal $U_y/P \propto j_y/P$ on the azimuth angle α measured for 6.6 and 21 nm QWs,

respectively. Here α is the angle between the light polarization plane and x -direction. In both cases the data are well fitted by $U_y(\alpha)/P = A + B \sin(2\alpha) + C \cos(2\alpha)$. While in 6.6 nm QWs such a current has not been detected so far, in 21 nm QWs it has been studied in a very details in Ref. [1] and demonstrated to be due to the photogalvanic effect [2, 3]. A particular feature of the photogalvanic effect in QWs of (013)-orientation orientation is that, in contrast to (001)-grown QWs, it can be excited at normal incidence of radiation. Quantum wells grown on the (013)-oriented substrate belong to the trivial point group C_1 lacking any symmetry operation except the identity. Hence, symmetry does not impose any restriction on the relation between radiation electric field and photocurrent components. The polarization dependence of the photocurrent in structures of the C_1 point-group symmetry for the excitation along the QW normal with linearly polarized light is given by [1]

$$j_x = \left[\chi_{xxy} \sin 2\alpha - \frac{\chi_{xxx} + \chi_{xyy}}{2} + \frac{\chi_{xxx} - \chi_{xyy}}{2} \cos 2\alpha \right] I\eta, \quad (4)$$

$$j_y = \left[\chi_{yxy} \sin 2\alpha - \frac{\chi_{yxx} + \chi_{yyy}}{2} + \frac{\chi_{yxx} - \chi_{yyy}}{2} \cos 2\alpha \right] I\eta, \quad (5)$$

where χ is the third rank photogalvanic tensor. Exactly this polarization dependence is observed in experiment, see Fig. 6. For C_1 -symmetry group all components of the tensor χ are linearly independent and may be nonzero. Consequently, even for a fixed light polarization, the CPGE photocurrent direction is not forced to a certain crystallographic axis. Moreover, it varies with temperature, radiation wavelength, etc [1].

MICROSCOPIC THEORY

We describe the electron states in HgTe/CdHgTe quantum wells in the isotropic $\mathbf{k}\cdot\mathbf{p}$ model following Ref. [4]. The Dirac cones in the QW of critical width are formed from the four states

$$\begin{aligned} |E1, +1/2\rangle &= f_1(z)|\Gamma_6, +1/2\rangle + f_4(z)|\Gamma_8, +1/2\rangle, \\ |H1, +3/2\rangle &= f_3(z)|\Gamma_8, +3/2\rangle, \\ |E1, -1/2\rangle &= f_1(z)|\Gamma_6, -1/2\rangle + f_4(z)|\Gamma_8, -1/2\rangle, \\ |H1, -3/2\rangle &= f_3(z)|\Gamma_8, -3/2\rangle, \end{aligned} \quad (6)$$

which are degenerate at $\mathbf{k} = 0$, with \mathbf{k} being the in-plane wave vector. Here $f_1(z)$, $f_3(z)$, and $f_4(z)$ are the envelope functions, which can be chosen real, z is the growth direction, $|\Gamma_6, \pm 1/2\rangle$, $|\Gamma_8, \pm 1/2\rangle$, and $|\Gamma_8, \pm 3/2\rangle$ are the basis functions of the Γ_6 and Γ_8 bands. At $\mathbf{k} \neq$

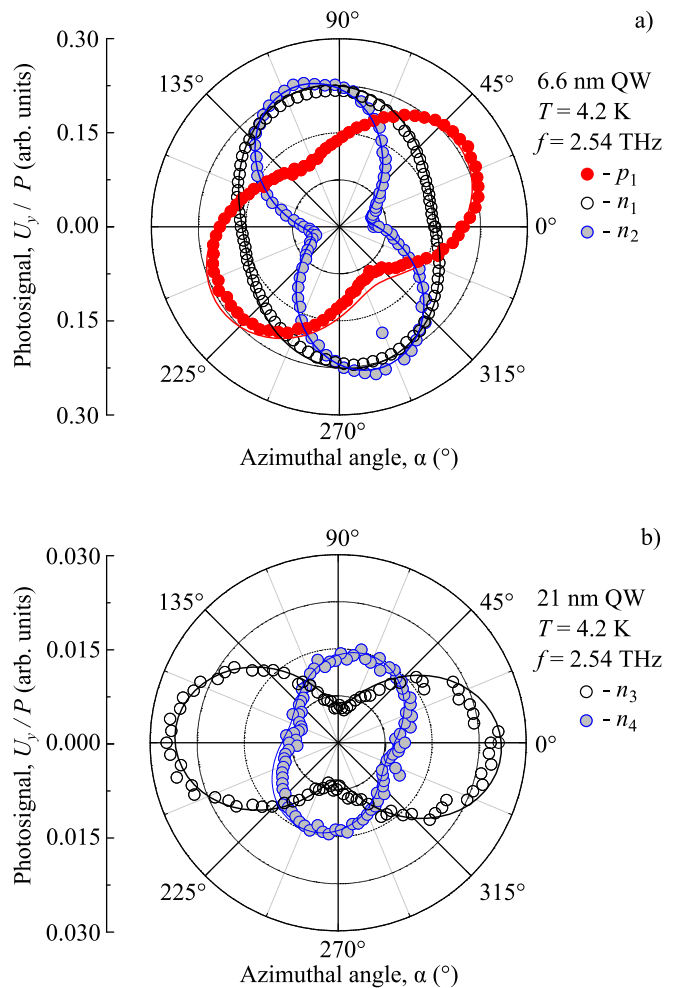


FIG. 6: Polarization dependence of the photovoltage normalized by radiation power, U_y/P , excited with normal incident radiation in (a) 6.6 nm and (b) 21 nm QWs at zero magnetic field. The normalized photosignal is shown for different carrier densities and fitted after $U_y(\alpha)/P = A + B \sin(2\alpha) + C \cos(2\alpha)$.

0, the states (6) are coupled that is described by the effective Hamiltonian

$$H = \begin{pmatrix} 0 & iAk_+ & 0 & 0 \\ -iAk_- & 0 & 0 & 0 \\ 0 & 0 & 0 & -iAk_- \\ 0 & 0 & iAk_+ & 0 \end{pmatrix} \quad (7)$$

where A is the (real) constant describing the in-plane velocity, $A \approx (P/\sqrt{2}) \int f_1(z)f_3(z)dz$, $P = i(\hbar/m_0)\langle S|p_z|Z\rangle$ is the Kane matrix element, and $k_{\pm} = k_x \pm ik_y$. The sign of A depends on the sign of $f_3(z)$, we take $A > 0$. Solution of the Schrödinger equation with the Hamiltonian (7) for positive energy $\varepsilon_k = Ak$ yields

two functions

$$\psi_{+, \mathbf{k}} = \frac{\exp(i\mathbf{k} \cdot \boldsymbol{\rho})}{\sqrt{2}} \begin{pmatrix} 1 \\ -i \exp(-i\varphi) \\ 0 \\ 0 \end{pmatrix}, \quad (8)$$

$$\psi_{-, \mathbf{k}} = \frac{\exp(i\mathbf{k} \cdot \boldsymbol{\rho})}{\sqrt{2}} \begin{pmatrix} 0 \\ 0 \\ 1 \\ i \exp(i\varphi) \end{pmatrix},$$

where $\varphi = \arctan(k_y/k_x)$ is the polar angle of the wave vector.

We consider (013)-grown QWs and chose the coordinate frame $x \parallel [100]$, $y \parallel [0\bar{3}1]$, and $z \parallel [013]$. In such coordinate system, the basis functions of the Γ_6 and Γ_8 bands can be presented in the form

$$\begin{aligned} |\Gamma_6, +1/2\rangle &= S \uparrow, \\ |\Gamma_6, -1/2\rangle &= S \downarrow, \end{aligned} \quad (9)$$

$$\begin{aligned} |\Gamma_8, +3/2\rangle &= -\frac{X' + i(Y' \cos \theta - Z' \sin \theta)}{\sqrt{2}} \uparrow, \\ |\Gamma_8, +1/2\rangle &= \sqrt{\frac{2}{3}}(Z' \cos \theta + Y' \sin \theta) \uparrow \\ &\quad - \frac{X' + i(Y' \cos \theta - Z' \sin \theta)}{\sqrt{6}} \downarrow, \\ |\Gamma_8, -1/2\rangle &= \sqrt{\frac{2}{3}}(Z' \cos \theta + Y' \sin \theta) \downarrow \\ &\quad + \frac{X' - i(Y' \cos \theta - Z' \sin \theta)}{\sqrt{6}} \uparrow, \\ |\Gamma_8, -3/2\rangle &= \frac{X' - i(Y' \cos \theta - Z' \sin \theta)}{\sqrt{2}} \downarrow, \end{aligned} \quad (10)$$

where S , X' , Y' , and Z' are the Bloch amplitude of the Γ_6 and Γ_8 bands, respectively, referred to the cubic axes $x' \parallel [100]$, $y' \parallel [010]$, and $z' \parallel [001]$, $\theta \approx 18.4^\circ$ is the angle between the $[001]$ and $[013]$ axes, and the symbols \uparrow and \downarrow denote the spin projections $+1/2$ and $-1/2$ onto the z axis, respectively.

The deformation interaction of electrons with acoustic phonons in zinc-blende-type crystals has both intra-band and interband contributions [5, 6]. The matrix elements of strain-induced interband coupling are given by $V_{S, X'} = \Xi_{cv} u_{y'z'}$, $V_{S, Y'} = \Xi_{cv} u_{x'y'}$, $V_{S, Z'} = \Xi_{cv} u_{x'y'}$, where Ξ_{cv} is the interband constant of the deformation potential and $u_{\alpha\beta}$ are the strain-tensor components used here in the primed coordinate system. Note, that $\Xi_{cv} \neq 0$ in non-centrosymmetric crystals only. The matrix elements of strain-induced intraband interaction are taken in the form $V_{S, S} = \Xi_c \text{Tr} u_{\alpha\beta}$, $V_{X', X'} = V_{Y', Y'} = V_{Z', Z'} = \Xi_v \text{Tr} u_{\alpha\beta}$, where Ξ_c and Ξ_v are the deformation-potential constants ($\Xi_v = a$ in the Bir-Pikus notation [7], the constants b and d are neglected for simplicity). Accordingly, the Hamiltonian of electron-phonon interaction in the basis of functions (9) and (10) has the form

$$V = \begin{pmatrix} V_c & V_{cv} \\ V_{cv}^\dagger & V_v \end{pmatrix}, \quad (11)$$

where $V_c = \Xi_c(\text{Tr} u_{\alpha\beta})I_2$, $V_v = \Xi_v(\text{Tr} u_{\alpha\beta})I_4$, I_2 and I_4 are the identity matrices 2×2 and 4×4 , respectively,

$$V_{cv}^\dagger = \Xi_{cv} \begin{pmatrix} -\frac{(u_{yz} - iu_{xz}) \cos 2\theta + (u_{zz}/2 - u_{yy}/2 + iu_{xy}) \sin 2\theta}{\sqrt{2}} & 0 \\ \sqrt{\frac{2}{3}}(u_{xy} \cos 2\theta + u_{xz} \sin 2\theta) & -\frac{(u_{yz} - iu_{xz}) \cos 2\theta + (u_{zz}/2 - u_{yy}/2 + iu_{xy}) \sin 2\theta}{\sqrt{6}} \\ \frac{(u_{yz} + iu_{xz}) \cos 2\theta + (u_{zz}/2 - u_{yy}/2 - iu_{xy}) \sin 2\theta}{\sqrt{6}} & \sqrt{\frac{2}{3}}(u_{xy} \cos 2\theta + u_{xz} \sin 2\theta) \\ 0 & \frac{(u_{yz} + iu_{xz}) \cos 2\theta + (u_{zz}/2 - u_{yy}/2 - iu_{xy}) \sin 2\theta}{\sqrt{2}} \end{pmatrix},$$

and the strain-tensor components $u_{\alpha\beta}$ are rewritten in the QW coordinate frame.

The dominant contribution to electron scattering is

given by the terms proportional to u_{zz} because the out-of-plane component q_z of the wave vector of the phonon involved is typically much larger than the in-plane com-

ponent q_{\parallel} . In this approximation, the matrix element of electron scattering from the state (s, \mathbf{k}) to the state (s, \mathbf{k}') , described by the wave functions (8), assisted by emission or absorption of a bulk acoustic phonon with the wave vector \mathbf{q} has the form

$$V_{s\mathbf{k}',s\mathbf{k}}^{(\pm)} = \mp i \frac{q_z}{2} \left[\frac{\hbar N_{\mathbf{q}}^{(\pm)}}{2\rho\Omega_{\mathbf{q}}} \right]^{1/2} \left[\Xi_c Z_{11} + \Xi_v (Z_{44} + e^{is(\varphi' - \varphi)} Z_{33}) - \frac{i \sin 2\theta}{2\sqrt{2}} \Xi_{cv} (e^{is\varphi'} - e^{-is\varphi}) Z_{13} \right] \delta_{\mathbf{k}', \mathbf{k} \mp \mathbf{q}_{\parallel}}, \quad (12)$$

where $N_{\mathbf{q}}^{(\pm)} = N_{\mathbf{q}} + (1 \pm 1)/2$, $N_{\mathbf{q}}$ is the phonon occupation number, ρ is the crystal density, $\Omega_{\mathbf{q}} = c_l q$ is the phonon frequency, c_l is the speed of sound, $Z_{ij} = \int_{-\infty}^{+\infty} f_i(z) f_j(z) \exp(iq_z z) dz$, and $s = \pm$ is the index enumerating the Dirac cones. The matrix elements (12) contain asymmetric terms which are responsible for the emergence of oppositely directed electron fluxes \mathbf{j}_s in the cones during the energy relaxation of heated electron gas.

To calculate the electron fluxes, we introduce the electron distribution function $f_{s\mathbf{k}} = \bar{f}_{s\mathbf{k}} + \delta f_{s\mathbf{k}}$, where $\bar{f}_{s\mathbf{k}}$ is the quasi-equilibrium function of the Fermi-Dirac type, $\delta f_{s\mathbf{k}}$ is the anisotropic part of the distribution function. It is assumed that the radiation absorption followed by electron-electron collisions forms the quasi-equilibrium electron distribution with the electron temperature T_e which is slightly higher than the crystal lattice temperature T_0 . The electron temperature can be found from the energy balance equation

$$\sum_{s, \mathbf{k}, \mathbf{k}'} W_{s\mathbf{k}',s\mathbf{k}}^{(\text{ph})} (\varepsilon_{\mathbf{k}} - \varepsilon_{\mathbf{k}'}) \bar{f}_{s\mathbf{k}} (1 - \bar{f}_{s\mathbf{k}'}) = I\eta, \quad (13)$$

where $W_{s\mathbf{k}',s\mathbf{k}}^{(\text{ph})} = (2\pi/\hbar) \sum_{\mathbf{q}, \pm} |V_{s\mathbf{k}',s\mathbf{k}}^{(\pm)}|^2 \delta(\varepsilon_{\mathbf{k}'} - \varepsilon_{\mathbf{k}} \pm \hbar\Omega_{\mathbf{q}})$ is the rate of electron scattering assisted by a phonon emission and absorption, scattering processes between states in different cones are neglected, I is the radiation intensity, and η is the free-carrier absorbance. The left-hand side of Eq. (13) describes the electron energy losses due to cooling by phonons while the right-hand side stands for the energy gain by the free-carrier absorption of radiation.

The electron fluxes are determined by the anisotropic part of the distribution function

$$\mathbf{j}_s = e \sum_{\mathbf{k}} \mathbf{v} \delta f_{s\mathbf{k}}, \quad (14)$$

where $\mathbf{v} = \nabla_{\mathbf{k}} \varepsilon / \hbar = v \mathbf{k} / k$ is the electron velocity. We consider that at low temperatures, relevant to the experimental conditions, the momentum relaxation of carriers

is limited by elastic scattering from static defects while the energy relaxation is governed by deformation interaction with bulk acoustic phonons. Accordingly, $\delta f_{s\mathbf{k}}$ can be found from the Boltzmann equation

$$\frac{e}{\hbar} [\mathbf{v} \times \mathbf{B}] \cdot \frac{d \delta f_{s\mathbf{k}}}{d\mathbf{k}} = \sum_{\mathbf{k}'} [W_{s\mathbf{k},s\mathbf{k}'}^{(\text{ph})} \bar{f}_{s\mathbf{k}'} (1 - \bar{f}_{s\mathbf{k}}) - W_{s\mathbf{k}',s\mathbf{k}}^{(\text{ph})} \bar{f}_{s\mathbf{k}} (1 - \bar{f}_{s\mathbf{k}'})] - \frac{\delta f_{s\mathbf{k}}}{\tau_p}, \quad (15)$$

where τ_p is the momentum relaxation time. The straightforward calculation shows that the electron fluxes in the cones have the form

$$j_{\pm, x} = \mp \frac{|e|v \sin 2\theta}{2\sqrt{2}} \frac{n_{\pm}}{n} \left(\frac{d}{dE_F} \frac{\omega_c \tau_p^2}{1 + (\omega_c \tau_p)^2} \right) \xi I\eta, \quad (16)$$

$$j_{\pm, y} = \mp \frac{ev \sin 2\theta}{2\sqrt{2}} \frac{n_{\pm}}{n} \left(\frac{d}{dE_F} \frac{\tau_p}{1 + (\omega_c \tau_p)^2} \right) \xi I\eta, \quad (17)$$

where n_{\pm} are the carrier densities in the cones, $n = n_+ + n_-$ is the total density, $\omega_c = |e|v^2 B / (cE_F)$ is the cyclotron energy, and

$$\xi = \frac{\int_{-\infty}^{+\infty} \Xi_{cv} Z_{13} (\Xi_c Z_{11} + \Xi_v Z_{33} + \Xi_v Z_{44}) q^2 dq}{\int_{-\infty}^{+\infty} [(\Xi_c Z_{11} + \Xi_v Z_{44})^2 + (\Xi_v Z_{33})^2] q^2 dq}.$$

Equations (16) and (17) are obtained assuming that $E_F \gg k_B T \gg \hbar\Omega_{\mathbf{q}}$ and $|n_+ - n_-| \ll n$.

-
- [1] B. Wittmann *et al.*, *Semicond. Sci. Technol.* **25**, 095005 (2010).
 - [2] S.D. Ganichev, E. L. Ivchenko, and W. Prettl, *Physica E* **14**, 166 (2002).
 - [3] E. L. Ivchenko and S.D. Ganichev, *Spin Photogalvanics in Spin Physics in Semiconductors*, ed. M.I. Dyakonov (Springer, 2008).
 - [4] B. A. Bernevig, T.L. Hughes and S.C. Zhang, *Science* **314**, 1757 (2006).
 - [5] G.E. Pikus, V.A. Marushchak, and A.N. Titkov, *Sov. Phys. Semicond.* **22**, 115 (1988).
 - [6] E. L. Ivchenko and S. A. Tarasenko, *JETP* **99**, 379 (2004).
 - [7] G.L. Bir and G.E. Pikus, *Symmetry and Strain-Induced Effects in Semiconductors* (Wiley, New York, 1974).